

Microwave-resonator-enabled broadband on-chip electro-optic frequency comb generation

ZHAOXI CHEN,^{1,3,†}  YIWEN ZHANG,^{1,†}  HANKE FENG,¹ YUANSONG ZENG,^{1,2} KE ZHANG,¹ AND CHENG WANG^{1,2,*} 

¹Department of Electrical Engineering, City University of Hong Kong, Kowloon, Hong Kong, China

²State Key Laboratory of Terahertz and Millimeter Waves, City University of Hong Kong, Kowloon, Hong Kong, China

³e-mail: zxchen4@cityu.edu.hk

[†]These authors contributed equally to this work.

*Corresponding author: cwang257@cityu.edu.hk

Received 25 October 2024; revised 9 December 2024; accepted 10 December 2024; posted 11 December 2024 (Doc. ID 546194); published 30 January 2025

Optical frequency combs play a crucial role in optical communications, time-frequency metrology, precise ranging, and sensing. Among various generation schemes, resonant electro-optic combs are particularly attractive for their excellent stability, flexibility, and broad bandwidths. In this approach, an optical pump undergoes multiple electro-optic modulation processes in a high- Q optical resonator, resulting in cascaded spectral sidebands. However, most resonant electro-optic combs to date make use of lumped-capacitor electrodes with relatively inefficient utilization of the input electrical power. This design also reflects most electrical power back to the driving circuits and necessitates costly radio-frequency (RF) isolators in between, presenting substantial challenges in practical applications. To address these issues, we present an RF circuit friendly electro-optic frequency comb generator incorporated with on-chip coplanar microwave resonator electrodes, based on a thin-film lithium niobate platform. Our design achieves more than three times electrical power reduction with minimal reflection at the designed comb repetition rate of ~ 25 GHz. We experimentally demonstrate broadband electro-optic frequency comb generation with a comb span of >85 nm at a moderate electrical driving power of 740 mW (28.7 dBm). Our power-efficient and isolator-free electro-optic comb source could offer a compact, low-cost, and simple-to-design solution for applications in spectroscopy, high-precision metrology, and optical communications. © 2025 Chinese Laser Press

<https://doi.org/10.1364/PRJ.546194>

1. INTRODUCTION

Optical frequency comb (OFC) generators play crucial roles in various applications, including optical communications [1–3], spectroscopy [4,5], timekeeping [6], precise ranging [7,8], and exoplanet detections [9], by providing excellent light sources with coherent and equally spaced spectral lines. Recent progress in photonic integrated circuits has paved the way for on-chip comb sources, with significantly improved compactness, efficiency, and scalability [10–14]. Integrated OFCs have been achieved based on various physical principles and material platforms, including mode-locked semiconductor lasers (e.g., in GaAs [15] and InAs [16]), optical Kerr nonlinearity (e.g., in SiN [17–19], AlN [20], and AlGaAs [21]), and electro-optic (EO) modulation (e.g., in LN [22–26] and Si [27]).

Among these schemes, electro-optic frequency combs are particularly attractive for their GHz repetition rates, broad tunability, and intrinsic mutual coherence [28,29]. An EO frequency comb is generated by modulating a continuous-wave

laser signal through one or multiple phase and amplitude EO modulators. This modulation process translates the input laser's single frequency into a comb of equally spaced frequency lines. Traditionally, this is often achieved using off-the-shelf modulators based on lithium niobate (LiNbO₃, LN), a material well known for its excellent optical properties and significant $\chi^{(2)}$ nonlinearity [30,31]. In recent years, the rapidly emerging thin-film LN (TFLN) platform, with tightly confined optical waveguides and substantially enhanced EO modulation efficiency [32–37], has further enabled integrated EO combs with much higher integration levels and wider comb spans compared with their bulk counterparts [38–40]. In particular, resonant EO combs that leverage optical resonators with ultrahigh quality (Q) factors have achieved remarkable comb spans, since the optical pump can be circulated and modulated for dozens of round trips. For example, an over 80 nm wide EO comb has been achieved in a TFLN optical resonator with a Q factor of 1.5×10^6 [24]. Further adopting a dual-resonator design has

pushed the optical conversion efficiency to 30% with an even wider comb span of 132 nm in wavelength [41].

To date, however, most on-chip resonant EO comb generators make use of a ground-signal-ground (GSG) capacitive electrode for applying the EO modulation signals [Fig. 1(a)]. This electrode configuration is essentially a lumped-capacitor load from the driving circuit perspective, where the input electrical power is almost fully reflected and not efficiently utilized. As a result, several watts of electrical driving power are often required for broadband EO comb generation (e.g., 2.2 W in Ref. [41] and 1 W in Ref. [42]). Moreover, the high reflected electrical power could be detrimental to the driving RF circuit, necessitating bulky and costly isolators or circulators to prevent power reflection to the electrical amplifier [Fig. 1(a)]. In short, the lumped-capacitor electrode design has become a major hurdle in terms of complexity, cost, and power consumption to the practical application of integrated resonant EO combs.

To address these issues, we propose and demonstrate an on-chip coplanar waveguide (CPW) microwave resonator electrode for efficient and RF circuit friendly driving of EO frequency combs. Compared with a conventional lumped-capacitor electrode, our device features a 3.6 times electrical field enhancement, which leads to more than three times reduction in power consumption with negligible electrical power reflection (-46 dB). Leveraging a 4-inch wafer-scale TFLN platform, we experimentally demonstrate broadband power-efficient EO frequency comb generation with a repetition rate of 25.6 GHz and a comb span exceeding 85 nm. Importantly, this is achieved using an optical racetrack resonator with a moderate $Q_L = 8.5 \times 10^5$, at a relatively low electrical driving power of 28.7 dBm, and without the use of electrical isolators or circulators. The design and analytical model can be readily extended

to other RF frequencies, supporting power-efficient EO comb generation with a wide range of target repetition rates.

2. DESIGN AND MODELING OF COPLANAR WAVEGUIDE RESONATOR ELECTRODE

Figure 1(c) illustrates the working principle of the proposed EO comb generator, consisting of an optical racetrack resonator fabricated in TFLN, integrated with CPW resonator electrodes. High-speed modulating electrical signal is applied to the input GSG microelectrodes, which is capacitively coupled into the CPW resonator by an interdigitated electrode (IDE). The CPW resonator consists of a GSG transmission line with a length equal to a quarter wavelength ($\lambda/4$) and shorted terminals on the opposite end, forming a quarter-wave resonator. When the applied microwave signal is near resonance frequency, the electrical field is significantly enhanced at the coupling (open) port, while the shorted end exhibits zero voltage (but finite current flow), following a sinusoidal $\lambda/4$ standing-wave pattern along the transmission line [Fig. 1(c)]. Through precise engineering of the IDE to achieve impedance matching between the microwave resonator and the driving circuit, the input electrical power can be critically coupled into the resonator, leading to enhanced EO modulation efficiency and negligible reflected electrical power.

A crucial requirement to achieve efficient EO comb generation is phase matching between the resonant optical- and micro-waves. In our device architecture, this is naturally satisfied when the microwave resonance frequency f_{MR} , the applied microwave frequency f_{MW} , and the optical free-spectral range (FSR) are equal. As the schematic shows in Fig. 1(c), considering a counter-clockwise-traveling optical pulse (green) present at the top middle section of the microwave resonator at time t_0 , it experiences a positive maximum EO modulation effect if the microwave field is pointing upwards (from signal to ground) at this point. The optical pulse circulates and reaches the bottom middle section of the resonator at time $t_0 + \tau/2$, where $\tau = 1/\text{FSR}$ is the round-trip time of the optical resonator. Although the electric field at this location is opposite to that in the upper gap [pointing downwards at time t_0 , as shown in Fig. 1(c)], it exactly flips to the upward-pointing direction at $t_0 + \tau/2$, as long as the microwave modulation frequency f_{MW} is equal to the optical FSR (such that microwave period $T_{MW} = 1/f_{MW} = \tau$). As a result, the optical pulse again sees a positive maximum EO modulation field at $t_0 + \tau/2$. At other locations of the resonator, although the electric field strength may be smaller, the optical signal always experiences upward-pointing electric field and therefore a constructive accumulation of EO modulation throughout the resonator.

In our device targeting a repetition rate of ~ 25 GHz, the microwave transmission line has an effective index ($n_{\text{eff},MW}$) of ~ 2.6 and an effective wavelength of 4.4 mm, leading to a total length of 1.1 mm for the $\lambda/4$ resonator. Meanwhile, the optical group index ($n_{g,O}$) is 2.26 in the TFLN waveguide at telecommunication wavelengths, necessitating a round-trip length of 5.1 mm for the racetrack resonator. We use a bending radius of approximately 80 μm with a Euler curve shape to minimize bending loss, such that the straight section of the racetrack is 2.3 mm long. This allows the $\lambda/4$ resonator to

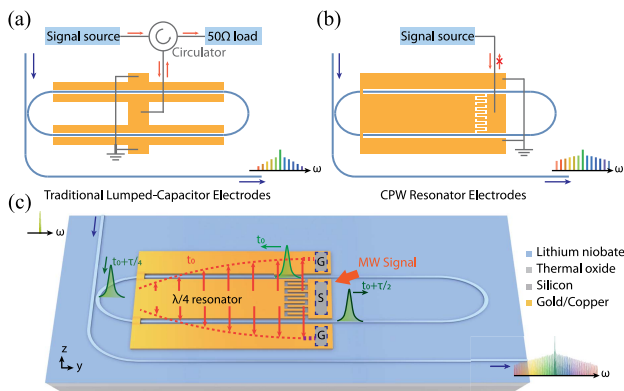


Fig. 1. Working principle of the microwave-resonator-enabled broadband EO comb generation process. (a), (b) Schematic comparison of EO comb generators with traditional lumped-capacitor design (a), where a circulator and an external 50 Ω load are needed to prevent electrical power reflection to the driving circuit, and the proposed $\lambda/4$ microwave resonator design (b). The microwave resonator serves both electrical field enhancement and prevention of electrical power reflection. (c) Schematic illustration of the electrical field distribution and phase-matching condition in the microwave-resonator-enhanced EO comb generator. Green pulses indicate the optical signal locations at different times t_0 , $t_0 + \tau/4$, and $t_0 + \tau/2$. Red arrows indicate electrical field distributions in the two gaps of the coplanar microwave resonator at t_0 , which would be reversed at $t_0 + \tau/2$.

be placed within the left half of the optical resonator to satisfy the phase-matching condition discussed above.

We design and finely tune the microwave resonator and coupling IDE to achieve impedance matching with the external driving circuit at the target resonance frequency. Figure 2(a) illustrates the top-view and cross-section schematic of the CPW microwave resonator. This short-circuit $\lambda/4$ resonator can be equivalently modeled by a parallel RLC resonant circuit near resonance [Fig. 2(b)], where the input signal is applied from the driving circuit (ii) into the resonator circuit (i). Assuming there is no extra loss on the transmission line, the total input impedance of (i) is given by

$$Z_{\text{in}} = \frac{1}{i\omega C_{\kappa}} + R_p + Z_{\text{LCR}} = \frac{1}{i\omega C_{\kappa}} + R_p + \left(\frac{1}{i\omega L} + i\omega C + \frac{1}{R} \right)^{-1}, \quad (1)$$

where C_{κ} represents the capacitance of the IDE, R_p is the parasitic resistance of the IDE, and R , L , and C are the equivalent resistance, inductance, and capacitance of the RLC resonator, respectively. Using conformal mapping techniques, the geometric contribution to capacitance C_l and inductance L_l per unit length of a CPW line can be expressed as [43,44]

$$C_l = 4\epsilon_0\epsilon_{\text{eff}} \frac{K(k_0)}{K(k'_0)}, \quad (2)$$

$$L_l = \frac{\mu_0}{4} \frac{K(k'_0)}{K(k_0)}, \quad (3)$$

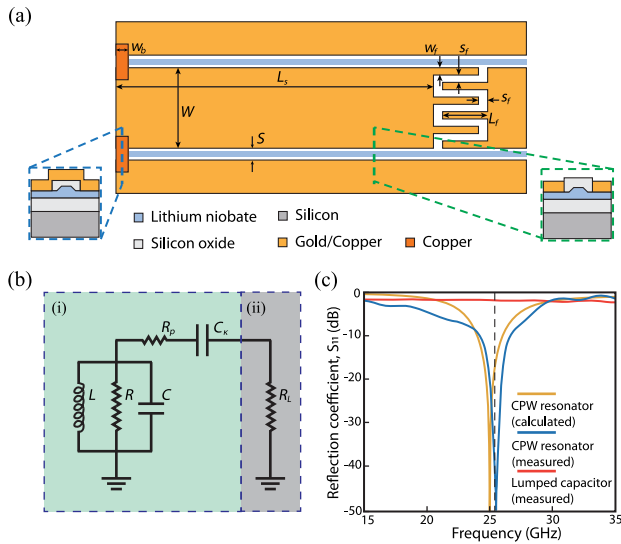


Fig. 2. Microwave resonator design. (a) Top view of the CPW resonator with shorted terminal at the left end and coupling interdigitated finger electrodes at the right-hand side. Insets: cross-section schematics of the CPW resonator at the shorted metallic bridge (blue dashed line) and in the middle of the resonator (green dashed line). (b) Equivalent circuit model of the short-circuited $\lambda/4$ CPW resonator (i), driven by an external circuit (ii) with a source impedance of $R_L = 50 \Omega$. (c) Calculated (yellow) and measured (blue) microwave reflection coefficients of the CPW resonator, and that measured from a lumped-capacitor electrode (red).

where ϵ_0 and μ_0 are the vacuum permittivity and permeability, respectively. ϵ_{eff} is the effective dielectric constant of the CPW mode spanning across air, LN, and top/bottom cladding, which is estimated to be 5.9 in our device. $K(k_0)$ and $K(k'_0)$ denote the complete elliptic integrals of the first kind, with the arguments

$$k_0 = \frac{W}{W + 2S} \quad \text{and} \quad k'_0 = \sqrt{1 - k_0^2}, \quad (4)$$

where $W = 155 \mu\text{m}$ is the signal width of the CPW line, and $S = 7 \mu\text{m}$ is the electrode gap. For nonmagnetic substrates and neglecting kinetic inductance, L_l is determined by the CPW geometry only, whereas C_l depends on both the geometry and ϵ_{eff} . The calculated values are $C_l = 1.15 \times 10^{-10}$ F/m and $L_l = 2.1 \times 10^{-10}$ H/m in our CPW line. The characteristic impedance is then given by

$$Z_0 = \sqrt{L_l/C_l}, \quad (5)$$

which results in a value of 42.8Ω for the current design. The corresponding total C and L values can then be calculated by multiplying with the length of the CPW line, $L_s = 1100 \mu\text{m}$:

$$C = L_s \times C_l \quad \text{and} \quad L = L_s \times L_l, \quad (6)$$

and the resistance R can be calculated using the characteristic impedance Z_0 :

$$R = \frac{Z_0}{\alpha L_s}, \quad (7)$$

where α is the loss coefficient of the transmission line. We obtain $\alpha = 0.11 \text{ mm}^{-1}$ by measuring a long CPW line with the same cross-section configuration, leading to an estimated $R = 350 \Omega$.

In our design, we intentionally set the characteristic impedance Z_0 of the isolated CPW resonator to be below $R_L = 50 \Omega$, since the total input impedance also includes the coupling capacitance C_{κ} and the parasitic resistance R_p of the IDE following Eq. (1), where the coupling capacitance C_{κ} can be obtained by

$$C_{\kappa} = C_{\text{unitcell}} \times L_f \times (n - 1). \quad (8)$$

Here L_f is the IDE finger length, n is the number of finger pairs, C_{unitcell} is the capacitance of each unit cell and can be calculated by

$$C_{\text{unitcell}} = 4\epsilon_c \frac{K(k_1)}{K(k'_1)} \quad \text{and} \quad k_1 = \frac{w_f}{w_f + 2s_f}, \quad (9)$$

where ϵ_c is the relative dielectric constant, $w_f = 3 \mu\text{m}$ is the finger width, and $s_f = 2 \mu\text{m}$ is the finger slot width in our design.

It should be noted that the existence of the coupling capacitor not only changes the input impedance Z_{in} , but also shifts the resonance frequency f_{MR} from the isolated RLC resonance. As a result, deviation in the coupling capacitance C_{κ} from the design value would cause undesirable impedance and frequency mismatch. In our experimental validation stage, we vary the IDE length L_f to achieve a near 50Ω input impedance at the target frequency to match that of the external driving circuit and minimize power reflection.

We experimentally verify the performance of the designed $\lambda/4$ resonator by measuring the reflection coefficient

$S_{11} = |(Z_{in} - R_L)/(Z_{in} + R_L)|$, which should ideally be zero at 25 GHz, using a vector network analyzer. Figure 2(c) displays the measured responses from a CPW resonator with an optimal finger length $L_f = 33.5 \mu\text{m}$ (blue), in comparison with that of a lumped-capacitor electrode (red). The fabricated resonator shows a strong resonance dip at 25.67 GHz, with an on-resonance reflection down to -49.8 dB . The measured results are also consistent with the calculation results from the equivalent circuit model (yellow), where the slight discrepancy may result from deviations in the geometric dimensions and dielectric constants between theory and actually fabricated devices. Importantly, the power reflection could remain $< -20 \text{ dB}$ (less than 1%) within a relatively broad frequency range of 1 GHz, which provides crucial tolerance and flexibility in practical applications where the optical FSR may not be perfectly aligned with the microwave resonance. In our actual device to be discussed in more details next, the EO comb operates at a repetition rate of 25.612 GHz (dashed line), where the power reflection is -46 dB . This is in sharp contrast to the lumped-capacitor case (red) with a -3 dB power reflection into the driving circuit (rest is lost in the on-chip resistance).

3. DEVICE FABRICATION

All devices are fabricated on *x*-cut TFLN wafers (NANOLN). The wafer stack consists of a 500 nm TFLN layer, a $4.7 \mu\text{m}$ thermal oxide buffer layer, and a 500 μm high-resistance silicon substrate layer. The TFLN wafer is first coated by a layer of 700 nm thick SiO_2 using plasma-enhanced chemical vapor deposition (PECVD) as etch mask. The optical waveguides and optical racetrack cavities are then patterned by an ASML UV stepper lithography system (NFF, HKUST). The patterns are transferred into the oxide mask layer and LN layer sequentially using reactive ion etching (RIE) with a 250 nm etch depth. After removing the remaining etch mask, another layer of PECVD oxide is coated to form a $1.5 \mu\text{m}$ thick upper cladding of the optical waveguides. The metallic electrodes (750 nm of copper, 50 nm of gold) are formed by a second stepper lithography process, followed by thermal deposition and lift-off. $5 \mu\text{m}$ wide metallic bridges (800 nm of copper) are then patterned at the short end of the CPW resonator by electron-beam lithography (EBL), thermal deposition, and lift-off processes. Finally, facets of the fabricated devices are cleaved for optical measurements. The fabricated optical bus (racetrack) waveguide has a top width of $1.2 \mu\text{m}$ ($2 \mu\text{m}$). Figure 3(a) shows the micrographs of the fabricated EO comb generators with lumped-capacitor (top, as a reference) and CPW resonator electrodes (bottom). Figure 3(b) shows scanning electron microscope (SEM) images with details of the metallic bridges and the IDE.

4. RESULTS AND DISCUSSION

We experimentally demonstrate power-efficient and RF isolator-free EO comb generation enabled by the CPW microwave resonator. An optical pump from a continuous-wave tunable laser (Santec TSL-550) is launched into the TFLN waveguide via a lensed fiber. The optical output is collected by another lensed fiber and recorded by an optical spectrum analyzer (Yokogawa AQ6370D). The driving microwave signal near

25 GHz is generated by an RF synthesizer and amplified by an electrical power amplifier. For the microwave resonator devices, the amplified electrical signal is applied directly onto the microelectrodes using a GSG probe, without the need of a circulator or isolator, thanks to the excellent impedance matching and minimal power reflection. As for the reference device with lumped-capacitor electrodes, the amplified electrical signal is first passed through a microwave circulator before being delivered to the microelectrodes. The reflected electrical power is then terminated at a 50Ω load through the circulator, similar to that used in Refs. [24,41]. To compensate for the loss from the circulator (0.9 dB at 25 GHz), the output power from an electrical amplifier is slightly higher than that used for measuring the CPW devices. During the experiments, the optical input pump power is fixed at 2 mW and the applied electrical driving powers on chip are calibrated to be 740 mW (28.7 dBm) in both cases.

Experimental results show that our CPW resonator enables frequency comb generation with an approximately doubled comb span from the reference lump-capacitor device. When the input optical and microwave frequencies are both tuned into resonance with the on-chip optical and microwave resonators, we achieve a broadband EO comb with an 85 nm span and 430 comb lines at a repetition rate of 25.612 GHz [Fig. 3(c) (ii)]. The measured spectral span and roll-off slope ($\sim 0.9 \text{ dB/nm}$) are both on par with that reported in Ref. [24] using a similar input RF power, but achieved with an optical resonator with 1.8 times lower loaded Q_L factor. Since the resonant EO comb span is proportionate to both optical Q_L and modulation index [45], this indicates an approximately 1.8 times increased electrical power efficiency. To better compare our results with earlier reports, we define a power efficiency figure of merit (FoM) based on the comb span normalized by square root of microwave power and loaded Q factor, as shown in Table 1. It can be seen that our electrical power utilization is significantly higher than that of all previously reported resonant EO comb generators.

The enhancement in modulation efficiency is further corroborated by comparing the measured EO comb with that of the reference device fabricated on the same chip, which features a comb span of 38 nm (narrower by a factor of 2.2) with a repetition rate of 25.255 GHz [Fig. 3(c) (i)]. Taking into account the slightly lower Q_L of 6.8×10^5 in the reference device, the effective modulation enhancement factor of our microwave resonator design is 1.8, which corresponds to more than three times reduction in electrical power consumption. Considering that the signal length (L_s) of the microwave resonator electrode is approximately half ($1100 \mu\text{m}$) of that in the lumped-capacitor device ($2300 \mu\text{m}$), we estimate that the average electric field strength in the EO modulation region is enhanced by a factor of 3.6 in the microwave resonator. The EO comb span could in principle be further broadened to $>150 \text{ nm}$ with an improved optical Q_L factor of 1.5×10^6 and a higher microwave power of 33.4 dBm [Fig. 3(c) (iii), same condition as that in Ref. [41]]. In this case, a more careful engineering of the waveguide dispersion will likely be required. We note though, operating in a moderate- Q -factor regime in this work also offers distinct advantages for practical applications, as the overall

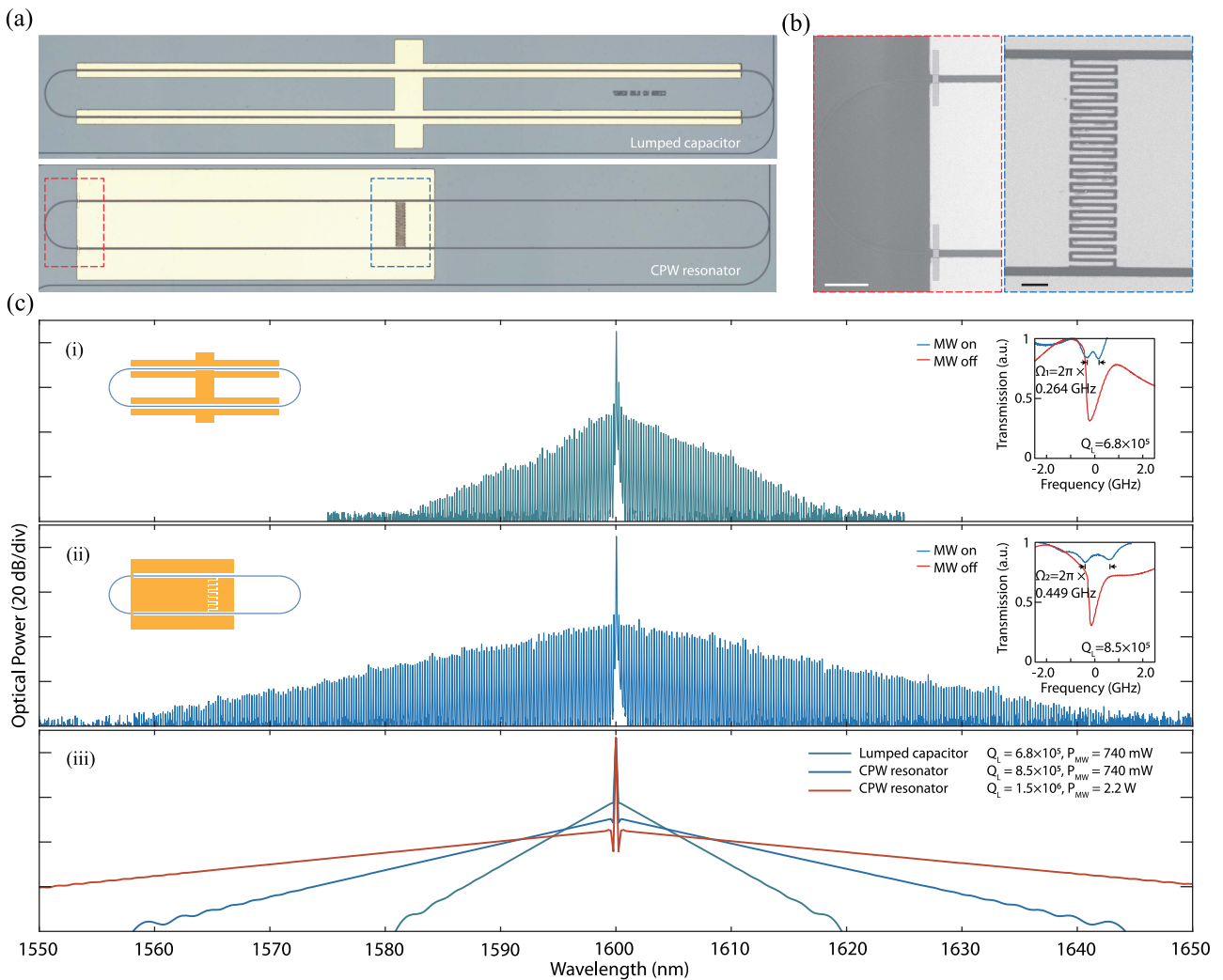


Fig. 3. Broadband EO comb generation. (a) Micrographs of the fabricated on-chip EO comb generators with lumped-capacitor (top) and CPW resonator (bottom) electrodes. (b) SEM images of the metallic bridges at the shorted terminal (left) and the IDE coupler (right). The scale bars are $20\ \mu\text{m}$ in both panels. (c) Measured EO comb spectra from the lumped-capacitor (i) and CPW resonator electrodes (ii) with the same input electrical power of $28.7\ \text{dBm}$. Insets show the device configurations (left) and measured optical transmission spectra (right) of the corresponding devices when microwave signal is off (red) and on (blue). The coupling rates $2\Omega_1 = 2 \times 2\pi \times 0.264\ \text{GHz}$ and $2\Omega_2 = 2 \times 2\pi \times 0.449\ \text{GHz}$ are measured under a moderate RF driven power of $5\ \text{dBm}$. (iii) Numerically simulated EO comb spectra of the current devices and setups shown in (i), (ii) and that of the current CPW resonator electrode design with potentially higher $Q_L = 1.5 \times 10^6$ and $P_{\text{MW}} = 2.2\ \text{W}$.

pump-to-comb conversion efficiency is higher ($\sim 0.6\%$, as compared to 0.3% in Ref. [24]) and the system is less prone to optical and microwave detuning.

Theoretically, our EO comb generator exhibits optimal performance when the microwave resonance frequency f_{MR} is perfectly matched with the optical FSR. To investigate the tolerance to potential mismatch between f_{MR} and FSR that may arise from fabrication deviations, we fabricate and measure a series of devices with identical microwave resonator electrodes but varying optical racetrack resonator sizes. The performance of each EO comb generator is evaluated by fixing the optical pump and microwave driving power, while finely tuning microwave frequency to the optical FSR in each device. As shown in Fig. 4, the generated comb span gradually decreases when the optical FSR shifts away from the CPW resonance frequency at

$25.67\ \text{GHz}$. The trend of measured comb span (blue dots) agrees well with the calculated relative electric field strength (black curve). Importantly, the measured comb span remains ($\sim 90\%$ the optimal value) within a relatively broad optical FSR range of $25.4\text{--}25.7\ \text{GHz}$, providing important robustness and tolerance in practical scenarios.

The design and analytical model of our CPW resonator can be readily extended to other frequencies. To showcase this scalability, we design and fabricate CPW resonator electrodes with a target resonance frequency near $10\ \text{GHz}$. To achieve this, the signal lengths L_s are set to $2990\ \mu\text{m}$ and $3000\ \mu\text{m}$, whereas the finger length L_f is optimized to $50\ \mu\text{m}$ for impedance match [Fig. 5(a)]. Figures 5(b) and 5(c) show the S_{11} parameter measured from the fabricated electrodes, where the resonance frequency locates at $9.82\ \text{GHz}$ and $9.67\ \text{GHz}$,

Table 1. Comparison of EO Frequency Comb Generators^a

Reference	Platform	Scheme	Microwave					Power Efficiency	
			Isolator/Circulator Needed	Span (nm)	Repetition Rate (GHz)	RF Driving Power	Optical Q_L (10^6)	FoM ($\text{nm} \cdot \text{W}^{-1/2}$ per Million Q_L)	
Zhang <i>et al.</i> [24]	TFLN	SR, LC	Yes	80	10.453	630 mW	1.5	67.2	
Rueda <i>et al.</i> [25]	LN	Microdisk, 3D copper cavity	No	11	8.9	100 mW	140	0.24	
Hu <i>et al.</i> [41]	TFLN	CR, LC	Yes	^b 132	30.925	2.2 W	^c 1.4	60	
Niu <i>et al.</i> [26]	TFLN	SR, LC	Yes	40	19.503	2 W	1.29	21.9	
Cai <i>et al.</i> [46]	TFLT	SR, LC	Yes	30	19.364	1 W	1	^d 30	
This work	TFLN	SR, CPW	No	85	25.612	740 mW	0.85	116	

^aSR, single resonator; LC, lumped-capacitor electrode; CR, coupled resonator; TFLT, thin-film lithium tantalate.

^bSpan defined at -70 dBm noise level.

^cIntrinsic quality factor of optical resonator cavity.

^dFrequency comb generation contains both Kerr and EO processes.

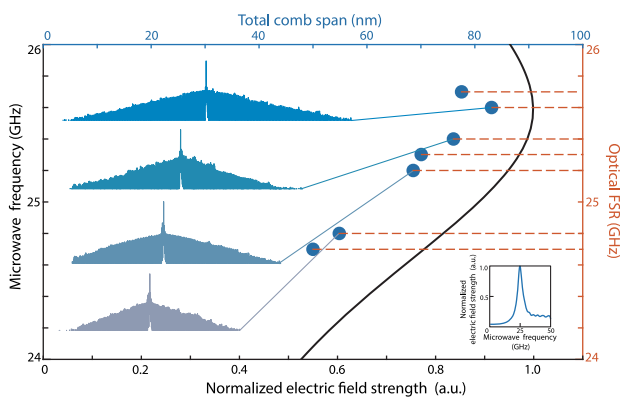


Fig. 4. Tolerance to frequency mismatch between optical and microwave resonators. Blue dots show the measured comb span (top horizontal axis) for optical racetrack resonators with different FSRs (right vertical axis), driven with microwave frequencies (left vertical axis) matched with FSR. The corresponding comb spectra are shown in the left insets. Black solid curve shows the normalized electric field strength (bottom horizontal axis) derived from the measured S_{11} parameter of the CPW resonator (S_{11} in the full measured frequency range is shown in the bottom right inset).

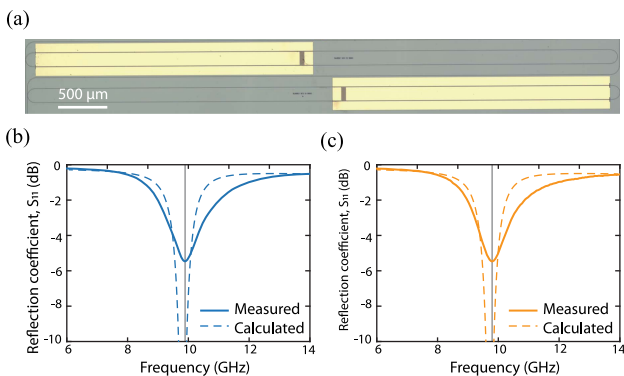


Fig. 5. Microwave resonator for different target frequencies. (a) Micrograph of CPW resonators targeting resonance near 10 GHz. (b), (c) Measured S_{11} parameter of the devices with $L_s = 2990 \mu\text{m}$ (b) and $L_s = 3000 \mu\text{m}$ (c). The dashed lines indicate the calculated results, and gray solid lines indicate resonance frequency at 9.82 GHz and 9.67 GHz.

respectively, proving excellent control over the resonance frequency. The relatively large power reflection may be attributed to undesirable resistance R_p caused by fabrication imperfections, leading to impedance mismatch and additional electrical power loss.

5. CONCLUSIONS

In conclusion, our EO comb source embedded with $\lambda/4$ CPW microwave resonator electrodes not only features substantially improved comb generation efficiency, but also strongly suppresses power reflection back to the driving circuit. The reduced RF power consumption and removal of electrical isolators or circulators are highly desired for such EO combs to be applied in practical and commercial scenarios. The design principles and analytical model developed in this work can be readily extended to other microwave frequencies (and in turn comb repetition rates) by scaling the CPW resonator and IDE lengths. Further improving the fabrication process to reduce metal surface roughness and applying micro-structured electrodes could be helpful in reducing microwave losses, thus achieving a higher modulation efficiency [47]. Our research provides a simple and feasible solution for achieving efficient and low-cost integrated EO frequency combs, promising for applications in precision metrology, advanced spectroscopy, and optical communication systems.

Funding. Research Grants Council, University Grants Committee (CityU 11212721, CityU 11204022, N_CityU113/20); Croucher Foundation (9509005); City University of Hong Kong (9610682).

Acknowledgment. We acknowledge Nanosystem Fabrication Facility (CWB) of HKUST for the device/system fabrication.

Disclosures. The authors declare no conflicts of interest.

Data Availability. Data underlying the results presented in this paper are not publicly available at this time but may be obtained from the authors upon reasonable request.

REFERENCES

- H. Hu and L. K. Oxenløwe, "Chip-based optical frequency combs for high-capacity optical communications," *Nanophotonics* **10**, 1367–1385 (2021).
- J. Pfeifle, V. Brasch, M. Lauer, *et al.*, "Coherent terabit communications with microresonator Kerr frequency combs," *Nat. Photonics* **8**, 375–380 (2014).
- V. Torres-Company, J. Schroder, A. Fulop, *et al.*, "Laser frequency combs for coherent optical communications," *J. Lightwave Technol.* **37**, 1663–1670 (2019).
- I. Coddington, N. Newbury, and W. Swann, "Dual-comb spectroscopy," *Optica* **3**, 414–426 (2016).
- N. Picqué and T. W. Hänsch, "Frequency comb spectroscopy," *Nat. Photonics* **13**, 146–157 (2019).
- S. B. Papp, K. Beha, P. Del'Haye, *et al.*, "Microresonator frequency comb optical clock," *Optica* **1**, 10–14 (2014).
- P. Trocha, M. Karpov, D. Ganin, *et al.*, "Ultrafast optical ranging using microresonator soliton frequency combs," *Science* **359**, 887–891 (2018).
- E. D. Caldwell, L. C. Sinclair, N. R. Newbury, *et al.*, "The time-programmable frequency comb and its use in quantum-limited ranging," *Nature* **610**, 667–673 (2022).
- M. G. Suh, X. Yi, Y. H. Lai, *et al.*, "Searching for exoplanets using a microresonator astrometry," *Nat. Photonics* **13**, 25–30 (2019).
- D. Liang and J. E. Bowers, "Recent progress in heterogeneous III-V-on-silicon photonic integration," *Light Adv. Manuf.* **2**, 59–83 (2021).
- H. Shu, L. Chang, Y. Tao, *et al.*, "Microcomb-driven silicon photonic systems," *Nature* **605**, 457–463 (2022).
- A. W. Elshaari, W. Pernice, K. Srinivasan, *et al.*, "Hybrid integrated quantum photonic circuits," *Nat. Photonics* **14**, 285–298 (2020).
- Y. Su, Y. He, X. Guo, *et al.*, "Scalability of large-scale photonic integrated circuits," *ACS Photon.* **10**, 2020–2030 (2023).
- A. Boes, B. Corcoran, L. Chang, *et al.*, "Status and potential of lithium niobate on insulator (LNOI) for photonic integrated circuits," *Laser Photon. Rev.* **12**, 1700256 (2018).
- S. Liu, X. Wu, D. Jung, *et al.*, "High-channel-count 20 GHz passively mode-locked quantum dot laser directly grown on Si with 41 Tbit/s transmission capacity," *Optica* **6**, 128–134 (2019).
- S. Pan, J. Huang, Z. Zhou, *et al.*, "Quantum dot mode-locked frequency comb with ultra-stable 25.5 GHz spacing between 20°C and 120°C," *Photon. Res.* **8**, 1937–1942 (2020).
- X. Xue, Y. Xuan, Y. Liu, *et al.*, "Mode-locked dark pulse Kerr combs in normal-dispersion microresonators," *Nat. Photonics* **9**, 594–600 (2015).
- M. H. P. Pfeiffer, C. Herkommer, J. Liu, *et al.*, "Octave-spanning dissipative Kerr soliton frequency combs in Si₃N₄ microresonators," *Optica* **4**, 684–691 (2017).
- J. Liu, E. Lucas, A. S. Raja, *et al.*, "Photonic microwave generation in the X- and K-band using integrated soliton microcombs," *Nat. Photonics* **14**, 486–491 (2020).
- H. Weng, J. Liu, A. A. Afridi, *et al.*, "Octave-spanning Kerr frequency comb generation with stimulated Raman scattering in an AlN microresonator," *Opt. Lett.* **46**, 540–543 (2021).
- L. Chang, W. Xie, H. Shu, *et al.*, "Ultra-efficient frequency comb generation in AlGaAs-on-insulator microresonators," *Nat. Commun.* **11**, 1331–1338 (2020).
- T. Ren, M. Zhang, C. Wang, *et al.*, "An integrated low-voltage broadband lithium niobate phase modulator," *IEEE Photon. Technol. Lett.* **31**, 889–892 (2019).
- M. Xu, M. He, Y. Zhu, *et al.*, "Flat optical frequency comb generator based on integrated lithium niobate modulators," *J. Lightwave Technol.* **40**, 339–345 (2022).
- M. Zhang, B. Buscaino, C. Wang, *et al.*, "Broadband electro-optic frequency comb generation in a lithium niobate microring resonator," *Nature* **568**, 373–377 (2019).
- A. Rueda, F. Sedlmeir, M. Kumari, *et al.*, "Resonant electro-optic frequency comb," *Nature* **568**, 378–381 (2019).
- R. Niu, S. Wan, W. Li, *et al.*, "An integrated wavemeter based on fully-stabilized resonant electro-optic frequency comb," *Commun. Phys.* **6**, 329–335 (2023).
- S. Liu, K. Wu, L. Zhou, *et al.*, "Microwave pulse generation with a silicon dual-parallel modulator," *J. Lightwave Technol.* **38**, 2134–2143 (2020).
- L. Chang, S. Liu, and J. E. Bowers, "Integrated optical frequency comb technologies," *Nat. Photonics* **16**, 95–108 (2022).
- A. Parriaux, K. Hammani, and G. Millot, "Electro-optic frequency combs," *Adv. Opt. Photon.* **12**, 223–287 (2020).
- Y. Dou, H. Zhang, and M. Yao, "Generation of flat optical-frequency comb using cascaded intensity and phase modulators," *IEEE Photon. Technol. Lett.* **24**, 727–729 (2012).
- R. Wu, V. Supradeepa, C. M. Long, *et al.*, "Generation of very flat optical frequency combs from continuous-wave lasers using cascaded intensity and phase modulators driven by tailored radio frequency waveforms," *Opt. Lett.* **35**, 3234–3236 (2010).
- C. Wang, M. Zhang, X. Chen, *et al.*, "Integrated lithium niobate electro-optic modulators operating at CMOS-compatible voltages," *Nature* **562**, 101–104 (2018).
- D. Zhu, L. Shao, M. Yu, *et al.*, "Integrated photonics on thin-film lithium niobate," *Adv. Opt. Photon.* **13**, 242–352 (2021).
- N. Chen, Y. Yu, K. Lou, *et al.*, "High-efficiency thin-film lithium niobate modulator with highly confined optical modes," *Opt. Lett.* **48**, 1602–1605 (2023).
- L. Shao, M. Yu, S. Maity, *et al.*, "Microwave-to-optical conversion using lithium niobate thin-film acoustic resonators," *Optica* **6**, 1498–1505 (2019).
- Q. Luo, F. Bo, Y. Kong, *et al.*, "Advances in lithium niobate thin-film lasers and amplifiers: a review," *Adv. Photon.* **5**, 034002 (2023).
- H. Feng, T. Ge, X. Guo, *et al.*, "Integrated lithium niobate microwave photonic processing engine," *Nature* **627**, 80–87 (2024).
- R. Cheng, X. Ren, C. Reimer, *et al.*, "Single-drive electro-optic frequency comb source on a photonic-wire-bonded thin-film lithium niobate platform," *Opt. Lett.* **49**, 3504–3507 (2024).
- K. Zhang, W. Sun, Y. Chen, *et al.*, "A power-efficient integrated lithium niobate electro-optic comb generator," *Commun. Phys.* **6**, 17–24 (2023).
- A. Boes, L. Chang, C. Langrock, *et al.*, "Lithium niobate photonics: unlocking the electromagnetic spectrum," *Science* **379**, eabj4396 (2023).
- Y. Hu, M. Yu, B. Buscaino, *et al.*, "High-efficiency and broadband on-chip electro-optic frequency comb generators," *Nat. Photonics* **16**, 679–685 (2022).
- I. L. Lufungula, A. Shams-Ansari, D. Renaud, *et al.*, "Integrated resonant electro-optic comb enabled by platform-agnostic laser integration," *Laser Photon. Rev.* **18**, 2400205 (2024).
- S. Gevorgian, L. P. Linner, and E. L. Kollberg, "CAD models for shielded multilayered CPW," *IEEE Trans. Microwave Theory Tech.* **43**, 772–779 (1995).
- M. Göppel, A. Fagner, M. Baur, *et al.*, "Coplanar waveguide resonators for circuit quantum electrodynamics," *J. Appl. Phys.* **104**, 113904 (2008).
- M. Kourogi, K. I. Nakagawa, and M. Ohtsu, "Wide-span optical frequency comb generator for accurate optical frequency difference measurement," *IEEE J. Quantum Electron.* **29**, 2693–2701 (1993).
- J. Cai, P.-Y. Wang, J. Li, *et al.*, "High-Q integrated lithium tantalate microring resonators for on-chip comb generation," *Opt. Lett.* **49**, 5921–5924 (2024).
- P. Kharel, C. Reimer, K. Luke, *et al.*, "Breaking voltage–bandwidth limits in integrated lithium niobate modulators using micro-structured electrodes," *Optica* **8**, 357–363 (2021).